Interaction of two parallel free oscillating flat plates and VIV of an upstream circular cylinder in laminar flow

Mohammad Jebelli, Mehran Masdari

Faculty of new sciences and technologies, University of Tehran, Tehran, Iran

Corresponding author: Mehran Masdari

Mailing address:

University of Tehran

Faculty of New Sciences and Technologies

North Kargar Street, Tehran, Iran

E-mail: m.masdari@ut.ac.ir

Abstract

Flow-induced vibration of bluff bodies and especially circular cylinders have been always of great interest and flat plates are known as useful means for altering flow structure to the desired condition. This work aims to investigate the effect of two parallel downstream flat plates which are mounted in the wake of a circular cylinder. Different configurations including eight horizontal ($0.5 \leq G \leq 4$) and two vertical gaps ($H=0.5$, 1) are numerically simulated to focus on the near wake structure and FIV of objects. The results show that the response of parallel plates in the wake of a stationary cylinder depends on both their horizontal and vertical locations. Change in the vertical distance alters the vortex shedding suppression mechanism. While a smaller vertical distance leads to a larger horizontal non-oscillating range, it comes with a higher maximum vibration amplitude. In the case of simultaneous oscillation, all three objects vibrate in all horizontal distances for the smaller vertical gap. The vibration disappears for the larger gap due to weaker interaction between the plates and the shear layers for a range of horizontal distances. The higher vibration amplitude in simultaneous vibration shows the considerable potential of the current concept for developing an improved energy harvesting system.

Keywords

Flow-Induced Vibration, Vortex shedding, Circular cylinder, Flat plate, Laminar flow

1 Introduction

Flow-induced motions have been of great interest in the past few decades. On one hand, it’s a concern for the reliability of different industrial structures with cylindrical components such as offshore rises, heat exchangers, and bridge cables and on the other hand, these types of phenomena are considered as a new source for clean and renewable energy with the growing shortage of fossil fuels and environmental concerns (Rostami and Armandei, 2017). FIMs are usually based on vortex formation and shedding around bluff bodies in which results in a periodic change in local pressure and consequently an asymmetric flow field around the body that applies an oscillatory force on it. This oscillatory force can be either from the upcoming vortices that result in a wake-induced motion or buffeting or induced to the object by its own vortex shedding, which causes Vortex-induced Vibration (VIV) (Armandei and Fernandes, 2016).

To develop the knowledge and gain a better insight into different aspects of these phenomena, extensive studies and reviews are performed and tremendous progress is achieved in the past decades on FIMs (Sarpkaya, 1979),(Sarpkaya, 2004),(Bearman, 1984),(Williamson and Govardhan, 2004). These studies can be divided into three main categories: understanding the phenomena, control, and suppression, or enhance and amplifying the motion. Primitive studies were devoted to understand the phenomena and to find a way to control or even suppress the motion because of their destructive effect. On the other hand, many studies have been carried out in the last decade to develop a system to harvest energy from wind and current as a renewable and clean source.

The various methods that are used to change the flow field and the response of the cylinders can be divided into two main categories: active and passive methods. While active methods generally require an external energy source and even a monitoring system, such as surface suction/blowing systems or rotating rods (Chen et al., 2013),(Zhu and Gao, 2017), passive ones try to achieve the desired condition by changing the geometry or adding some devices which are generally less costly and easier to install (Zhu and Yao, 2015),(Quadrante and Nishi, 2014),(Sui et al., 2016),(Assi et al., 2014).

Among the various approaches implemented to either suppress or amplify the FIMs, utilizing flat plates is known as a simple and also effective way to modify the flow field and the response of the objects to the desired conditions. Therefore, various arrangements of a circular cylinder as a bluff body and attached or detached flat plates have been extensively studied in the past decades.

The first studies on the effect of installing a flat plate to the rear end of a fixed circular cylinder date back to 1954. In this configuration, the flat plate works as a flow splitter, stabilizing and narrowing the wake, making a delay in vortex shedding, reducing the Strouhal number and drag coefficient (Roshko, 1954)(Gerrard, 1966)(Apelt et al., 1973). The plate length also has a significant effect and a large enough one may completely suppress vortex shedding (Kwon and Choi, 1996). The structure of the plate and connection angle to the cylinder are also effective to control the vortex shedding (Ozkan et al., 2017). This passive control mechanism also works in cylinders with elliptical cross sections (Soumya and Prakash, 2017).

Detached plates have also been used to change the wake and control vortex shedding. This configuration can also change the base pressure, Strouhal number, and even suppress vortex shedding, but its effectiveness depends on the horizontal and vertical position of the plate. A single and even parallel plates have been shown to be effective in reducing the drag coefficient (Ozono, 1999)(Hwang et al., 2003)(Dehkordi and Jafari, 2010). It can be concluded that while both of the attached and detached plates are useful to control devices for cylinders and are able to make a delay in vortex shedding and even completely suppress it, the detached plates' effectiveness is strongly more dependent on their length and location.

In 1990, Kawai studied the effect of an attached splitter plate on the free vibration of a circular cylinder and showed that this configuration leads to galloping associated with a high amplitude of vibration and a low frequency (Kawai, 1990). While a bare circular cylinder can only be vortex-excited, it can gallop in the presence of a splitter plate of sufficient length. This finding can be applied to any bluff body regardless of whether its cross section is sharp-edged or smooth (Nakamura et al., 1994). An increase in plate length leads to a transition from VIV to galloping regardless of whether the plate is simple or slotted (Stappenbelt, 2010)(Assi and Bearman, 2015). It is worth noting that a hinged plate can also suppress VIV, especially at low reduced velocities (Wu et al., 2014). Based on the splitter length, Liang et al. divided the cylinder response into four groups: VIV, the interaction between VIV and galloping, a combination of the velocity-restricted excitation and the interaction of VIV and galloping (Liang et al., 2018). Sun et al. in an attempt to find the reason for the transition between VIV and galloping found that the lift components generated by the splitter and the cylinder behave as the driving force and the suppressing force of galloping, respectively. Therefore, it can be said that the transition is a result of the competition between these forces (Sun et al., 2020). Utilizing a wavy plate with a proper length instead of a flat one, may suppress effectively the initial and lower branches of VIV and stir the galloping at high reduced velocities (Zhu and Liu, 2020). A single downstream splitter alleviates VIV at low reduced velocities while exciting the galloping at higher velocities. On the other hand, an upstream splitter delays vortex shedding and makes the wake narrower. Zhu et al. also found that using simultaneous oscillation can also completely suppress galloping (Zhu et al., 2020).

In general, it can be said that the use of flat plates to control vortex shedding and flow-induced motions, whether attached or not, has different and sometimes contradictory effects on the response of the system, and the length, stiffness, location, and type of connection are the main effective parameters.

As mentioned earlier, by the growing shortage of fossil fuels and environmental concerns, FIMs are considered as a new source of clean and renewable energy, especially in the last decade. Therefore, some studies have focused on harvesting energy from different configurations of a cylinder and a plate. The use of a piezoelectric plate attached to the rear side of a cylinder is known as a popular method for developing an energy harvesting system and has been investigated in several studies. VIPEC is a novel method proposed by An et al. in which vortex-induced pressure difference acts on a plate and drives it to squeeze piezo patches to convert the dynamic energy of fluid into electrical energy (An et al., 2018).

Wang et al. numerically studied the flow-induced vibration of a piezoelectric flexible plate behind a fixed cylinder. They found that the result of the system can be divided into suppression or VIV depending on the gap size and the plate length. The medium spacing with the smallest bending stiffness result in the maximum vibration amplitude (Wang et al., 2018a, 2018b). Armandei and Fernandes elastically mounted a flat plate with a rotating degree of freedom in the wake of a modified cylinder to extract marine current energy through buffeting. They found that although the buffeting response is independent of the horizontal gap, its efficiency strongly depends on the position of the elastic axis and the spring stiffness (Armandei and Fernandes, 2016). These results confirm that the wake of a bluff body can be considered as a source of energy, but a proper configuration is essential for higher efficiency.

Based on the above literature, it can be concluded that while the flat plates are widely used to control and suppress the FIMs, they are also noticed as a means to enhance the motion of the cylinder and even to harvest energy directly. On the other hand, small changes in length, location, and degree of freedom can significantly change the response of the system and there are still unknown aspects in the interaction between a plate and a circular cylinder.

In the present study, the FIMs of a combination of a circular cylinder and two parallel flat plates have been numerically studied in a laminar flow regime. Different configurations for the plates, which are mounted in the wake, including 8 horizontal and 2 vertical spacing are investigated to achieve a better understanding of vibrating plates. Simulations are also performed for simultaneous independent vibration of all three objects to find out the flow structure and response of the system.

Nomenclature

A	Plunging Amplitude
D	Circular Cylinder Diameter
L_P	Flat Plate Length
G	Non Dimensional Horizontal spacing
H	Non Dimensional Vertical spacing
m*	Mass Ratio
ζ	Damping Factor
CL	Lift Coefficient
CL_{rms}	Root Mean Square of Lift Coefficient
CD_{mean}	Mean Drag Coefficient
Cp	Pressure Coefficient
Cp_b	Base Pressure Coefficient
f	Plunging Oscillation Frequency
f_n	Transverse Natural Frequency
F_n	Non-dimensional Natural Frequency
ρ	Fluid Density
m	Body Mass
m_A	Added Mass
K	Transverse Stiffness Factor
U_{in}	Free Stream Velocity
U_r	Reduced Velocity
t	Physical Time
T	Non Dimensional Time
St	Strouhal number
$\dot{e}$	Energy Transfer rate

2 Problem description and CFD model

In this section, the problem is described in detail and the governing equation with the numerical method used for the simulations are presented.

2.1 Problem description

In the present study, the flow-induced vibration of a circular cylinder and two parallel flat plates mounted in wake is modelled by a mass-spring system with one degree of freedom proposed by Facchinetti et al. (Facchinetti et al., 2004). In Figure 1, a schematic representation of the flow passing objects that are elastically mounted perpendicular to the uniform flow is presented.

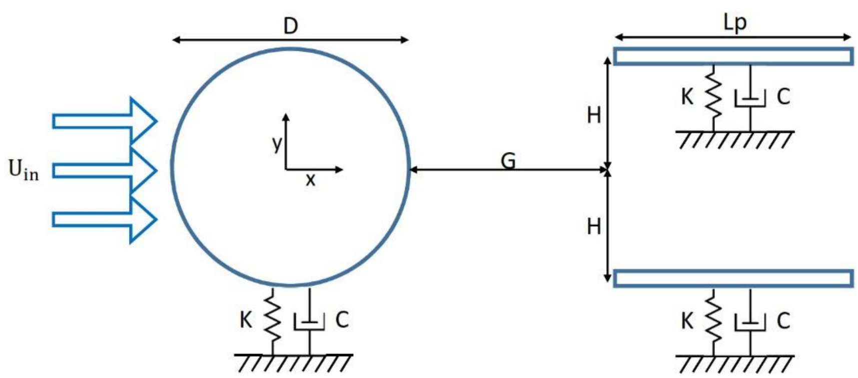

Figure 1 - Schematic diagram of flow past a free to oscillate cylinder and two parallel flat plate in tandem arrangement

'G' and 'H' represent the distance between the objects in streamwise and cross flow directions respectively. The diameter of the cylinder and the length of the plates are represented by 'D' and 'L_p', which are the same in the present study, and the thickness of the plates is set as δ=0.03D.

The Reynolds number, the mass, and the damping ratio are known as the main parameters in FIVs and play an important role in the dynamic response of the system. The mass ratio is defined as $m^* = m/m_A$ based on the mass of the body, and its added mass. Damping ratio can also be defined as $\zeta = c\ /\ (2\sqrt{mk})$, where C and K are the damping and spring stiffness of the system.

The wake transition of a circular cylinder occurs when Re is larger than 180 (Charles H K Williamson, 1996)(C H K Williamson, 1996)(Jiang et al., 2016), Therefore selecting higher Re numbers requires a three-dimensional simulation which is more applicable for engineering cases. This type of simulation, although very limited in number, provides a lot of information about the flow field and VIV mechanism (Nguyen and Nguyen, 2016)(Ishihara and Li, 2020; Li and Ishihara, 2021a). On the other hand, 3D simulations are extremely time-consuming and may not be proper to be conducted in a large number of configurations like those of the current study.

Therefore, to avoid three-dimensionality effects, a Reynold number of 100 (Based on the cylinder diameter 'D' and free stream velocity 'U_{in}') is selected for all of the cases that allows the utilization of a two-dimensional (2D) simulation method.

Since the main objective of the present study is to determine the effects of horizontal and vertical location of the parallel plates on the wake structure and response of the system, the mass ratio and Re number are kept constant at 10 and 100, respectively. The dimensional natural frequency of all objects is set based on the Strouhal number and the vortex shedding frequency of a bare fixed circular cylinder at Re=100, which are taken from references. The structural damping is also set to zero to encourage a high vibration amplitude. The non-dimensional parameters of the simulation are summarized in the Table 1 in which U_r is the reduced velocity and can be defined as U_{in}/f_nD.

According to the references (Prasanth and Mittal, 2008),(Kumar et al., 2018), the non-dimensional natural frequency which can be defined as $F_n = f_n D/U$ changes to $F_n = 16.6/Re$ for the current study. The reduced velocity can also be redefined as $U_r = 1/F_n$. Therefore, the non-dimensional natural frequency and the reduced velocity will be equal to $F_n = 0.166$ and $U_r = 6$, respectively for a Re number of 100.

Parameter	symbol	value
Mass ratio	m*	10
Damping ratio	ζ	0
Horizontal distance	G=L/D	0.5-0.4
Vertical distance	H=L/D	0.5, 1
Reynolds number	Re	100
Reduced velocity	U_r	6

Table 1 - Main Simulation Parameters

2.2 Governing Equations

The flow around the objects is modeled according to the conservation law of mass and momentum and is governed by the 2D incompressible, unsteady Navier-Stokes equations (NS) as follows (White, 1994):

$$\nabla.(u - \hat{u}) = 0 \qquad (1)$$

$$\rho\left(\frac{\partial u}{\partial t} + (u - \hat{u}).\nabla u + \right) = -\nabla P + \mu \nabla^2 u \qquad (2)$$

In above equations ρ, u, $\hat{u}$ and P are the fluid density, velocity vector, mesh velocity vector and pressure, respectively. The mechanical response of the objects are modelled by the mass-spring-damping system with considering one degree of freedom in crossflow direction. The non-dimensional equation is given as follow:

$$\ddot{Y} + \frac{4\pi\zeta}{u_r}\dot{Y} + \frac{4\pi^2}{U_r^2}Y = \frac{2C_L}{\pi m^*} \qquad (3)$$

Where $\ddot{Y}$, $\dot{Y}$ and Y represent transverse displacement, velocity and acceleration of the objects normalized by D (or L for the plates), $U_\infty$and U_∞^2, respectively. The C_L representing the instantaneous lift coefficient defines as:

$$C_L = \frac{F_Y}{0.5\ \rho\ U_\infty^2 D} \qquad (4)$$

The F_Y which is the transverse force component contains the effect of both pressure and viscose forces. The SIMPLE algorithm is used for coupling between the pressure and the velocity vector and the second-order upwind and the least-squares cell-based schemes are used for discretization of the convective and gradient terms, respectively.

2.3 Numerical Method

In order to numerically simulate the flow field, the ANSYS Fluent is utilized as a reliable CFD software. Since the objects in an FIV case start to oscillate, a dynamic mesh is required to change the grid at each time step. ANSYS Fluent employs an Arbitrary Lagrangian-Eulerian (ALE) algorithm that includes three dynamic mesh schemes, namely smoothing, layering and remeshing. For the current study, a diffusion-based smoothing method is used and a User-Defined Function (UDF) in C programming language is employed to solve the system response.

The size of the computational domain, and in particular the blockage effect, are of great importance in numerical simulations. Choosing a small domain can lead to an error in the prediction of the forces and the response of the system. On the other hand, an oscillating cylinder includes a larger wake compared to a fixed cylinder, so blockage is likely to play an even more important role.

The blockage of more than 2.5% for a circular cylinder can lead to hysteresis in the response of the object at the onset of synchronization in a laminar flow regime similar to that of this study (m^*= 10, Re =100). For the case of VIV of two circular cylinders in tandem and staggered arrangement, setting the lateral boundaries at a distance of 25D from the upstream cylinder (Equivalent to 2% of blockage) seems proper (Prasanth et al., 2006),(Prasanth and Mittal, 2008),(Prasanth and Mittal, 2009).

Figure 2 shows the size of the domain, the geometry of the model, and the boundary conditions used for the current study. The size of the whole computational domain is 75D×50D and the center of the cylinder is set as the origin of the coordinate system. The upstream and lateral boundaries are located 25D from the center of the cylinder and to accurately capture the wake, the downstream boundary is located 50D from the origin.

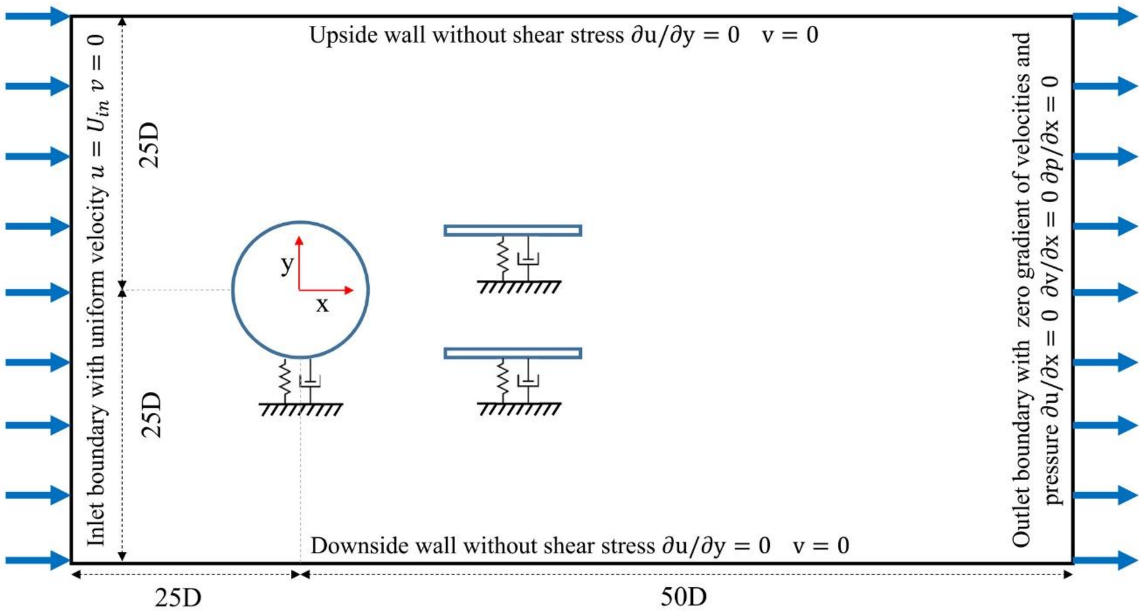

Figure 2 - Schematic of CFD model around a circular cylinder and two wake parallel plates including domain and boundary condition

The inlet boundary is imposed with a uniform velocity boundary. For the upper and lower bounds, the normal component of the velocity and the component of the stress vector along the boundary are equal to zero. At the outlet, a zero normal gradient is specified for the velocity and the pressure is specified with a reference value of zero. Finally, the surface of the cylinder and parallel plates are assumed to be smooth, with a no-slip boundary condition.

2.4 Computational domain and mesh dependency

Prior to the detailed study of the main cases, grid dependency and temporal resolution validation are performed to obtain an independent solution method.

The grid generated to simulate the flow around a circular cylinder and two parallel downstream plates is shown in Figure 3:

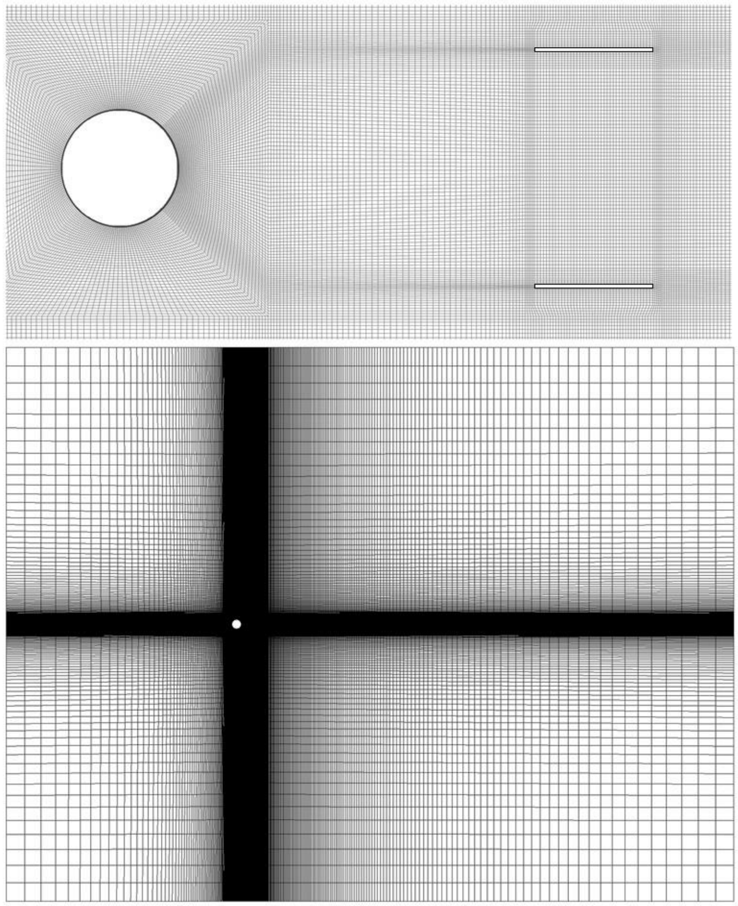

Figure 3 - Typical mesh elements in CFD model. up) around the cylinder and plates, down) the whole simulation domain

The grid around the surface of the cylinder has been divided into four parts: front, top, bottom, and the rear side which the last one is more important due to the presence of the parallel plates and high flow gradients. In order to reduce the computational cost, the mesh is also gradually coarsened in the regions far from the objects.

The grid dependency study was performed for two configurations. The first case includes a pair of a fixed circular cylinder and a flat plate mounted in the wake, and the second case is the 2DOF VIV of a bare circular cylinder. In both configurations, the grids are generally similar, but the second one contains more cells in the wake due to the parallel plates and the complexity of the flow.

Table 2 presents the variation of the normalized mean inline and maximum cross-flow amplitudes, Strouhal number, and mean drag coefficient of the VIV of a cylinder with 2DOF at Re=100. A convergence of the results can be seen in the case of G-1-2 with 200 nodes uniformly distributed on the cylinder surface.

Grid	Nodes on cylinder	X_{mean}	Y_{max}	St	Cd_{mean}
G-1-1	4×40	0.116	0.656	0.1634	1.986
G-1-2	4×50	0.115	0.647	0.1635	2
G-1-3	4×60	0.1151	0.645	0.1635	1.997

Table 2 – mesh independency study for 2D VIV of circular cylinder (Re=100, Ur=6.02)

For the second case of grid independence study, new grids with similar structures but more cells in the wake are utilized. Corresponding results are presented in Table 3.

Grid	Cylinder Nodes	Cylinder				Flat Plate			
		Cl_{max}	Cl_{rms}	St	CD	Cl_{max}	Cl_{rms}	St	CD
G-2-1	3×50+50	0.41	0.288	0.157	1.311	1.245	0.87	0.157	0.0782
G-2-2	3×50+60	0.405	0.288	0.157	1.310	1.254	0.875	0.157	0.0795
G-2-3	3×50+70	0.405	0.286	0.157	1.310	1.257	0.883	0.157	0.0799
G-2-4	3×50+80	0.405	0.285	0.157	1.309	1.258	0.884	0.157	0.0798

Table 3 - Mesh resolution sensitivity examinations for a stationary cylinder and a flat plate in G=3D at Re=100

A grid with 40% more cells on the rear side of the cylinder (G-2-3) ensures that the results are independent of the grid resolution. Therefore, this grid is chosen for further simulations with a fixed or oscillating combination of a cylinder and parallel flat plates. A temporal resolution analysis is also conducted on this grid for several time steps and a non-dimensional time step of $\Delta t = 0.002$, is found to be sufficiently small to assure independency.

3 Model validation

This section aims to provide a validated computational approach. Four cases, including a stationary bare cylinder, a cylinder, and a flat plate mounted in the wake, a cylinder and two parallel downstream flat plates, and finally the VIV of a cylinder with 2 DOF are selected to check the validation. The simulation domain is the same for all cases. In Table 4, the flow characteristics of the first case are presented and compared with other studies.

Author	CD	St	CL_{rms}	$-Cp_b$
(Park et al., 1998)	1.33	0.165	0.235	0.725
(Kravchenko and Moin, 1998)	1.32	0.164	0.222	0.73
(Stålberg et al., 2006)	1.32	0.166	0.233	-
(Posdziech and Grundmann, 2007)	1.325	0.1644	0.228	0.709
(Li et al., 2009)	1.336	0.164	-	0.701
(Qu et al., 2013)	1.319	0.1648	0.225	0.709
Present study	1.34	0.165	0.232	0.71

Table 4 - Comparison of flow quantities with the results of earlier studies for a stationary cylinder at Re= 100

The agreement between the current results and previous references confirms the validity of the simulation method for this case. For the second case, the change in Strouhal number and drag coefficient of the circular cylinder and a wake-mounted splitter plate is shown in Figure 4 and Figure 5.

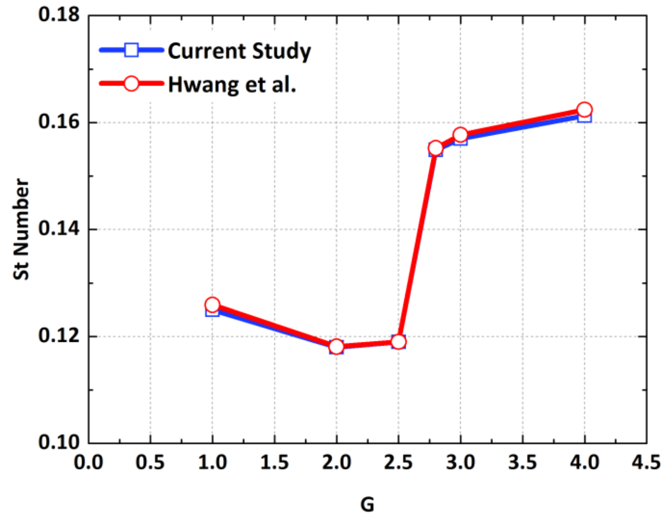

Figure 4 - Comparison of Strouhal number for different spacing in Re=100 (Hwang et al., 2003)

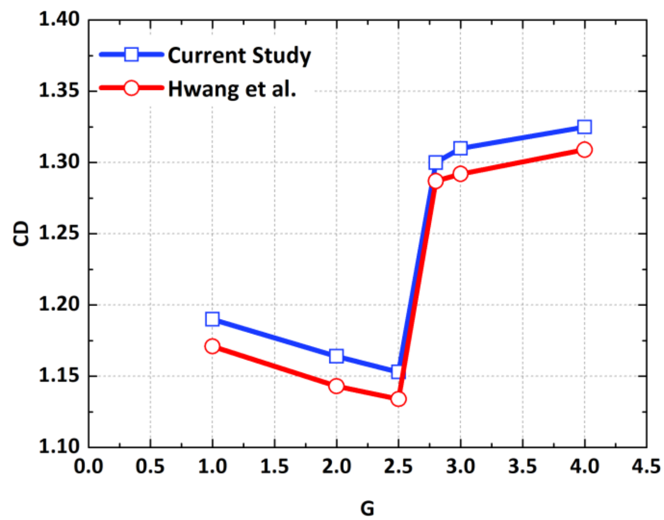

Figure 5 - Comparison of drag coefficient for different spacing in Re=100 (Hwang et al., 2003)

In this case, there is also good agreement and small deviations in the drag coefficient are negligible. According to the results, the presence of the plate alters the wake structure for G≤2.5 and significantly decreases the drag coefficient and the Strouhal number. For G≥2.8, regular vortex shedding appears and both parameters jump to higher values close to those of a bare cylinder.

For the third case, the variation of drag coefficient of a stationary cylinder and parallel downstream flat plates are compared with the results of (Dehkordi and Jafari, 2010) and presented in Figure 6.

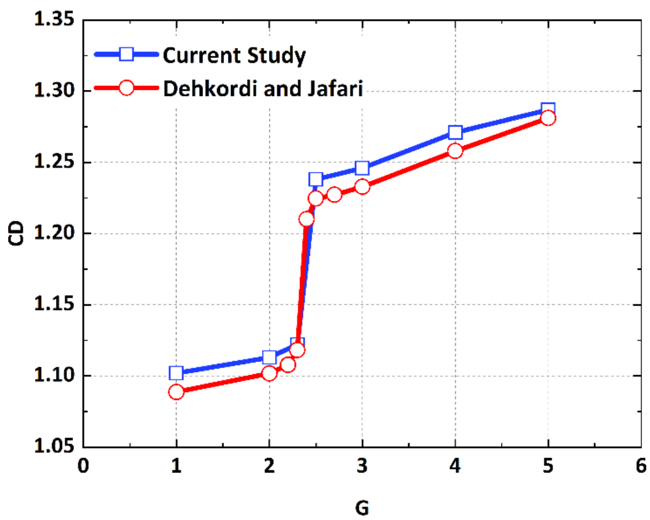

Figure 6 - Comparison of drag coefficient of the cylinder with dual downstream flat plates for different spacing in Re=100 (Dehkordi and Jafari, 2010)

In this case, the parallel plates are mounted with a fixed vertical spacing of H=0.75 and the horizontal spacing varies for 1<G<5. Small discrepancies between the results confirm that the numerical method is also capable of predicting the flow field between the objects and the effect of downstream plates on the upstream cylinder.

To examine the accuracy of the numerical method, the final validation case is the 2 DOF VIV of a circular cylinder. The results of the current simulation are compared with some previous studies in Table 5.

Author	Y_{max}	X_{mean}	St	CL_{max}	CD_{mean}	CD_{rms}
(Prasanth and Mittal, 2008)	0.53	0.1115	0.1643	0.1929	1.90	0.2486
(He et al., 2012)	0.503	0.1082	0.1652	0.1985	1.81	0.2244
(Tu et al., 2015)	0.525	0.1307	0.1652	0.2220	1.88	0.2664
Present study	0.54	0.110	0.1640	0.235	1.88	0.2660

Table 5 - Comparison of the results of the current study with previous studies for 2D VIV of a circular cylinder at Re= 100

The good agreement confirms the reliability of the numerical approach. Figure 7 presents the variation of the maximum amplitude of the cylinder for a range of Re numbers. It can be seen that the results agree well with those of Prasanth and Mittal (Prasanth and Mittal, 2008) (Decreasing case) and Tu et al. (Tu et al., 2015).

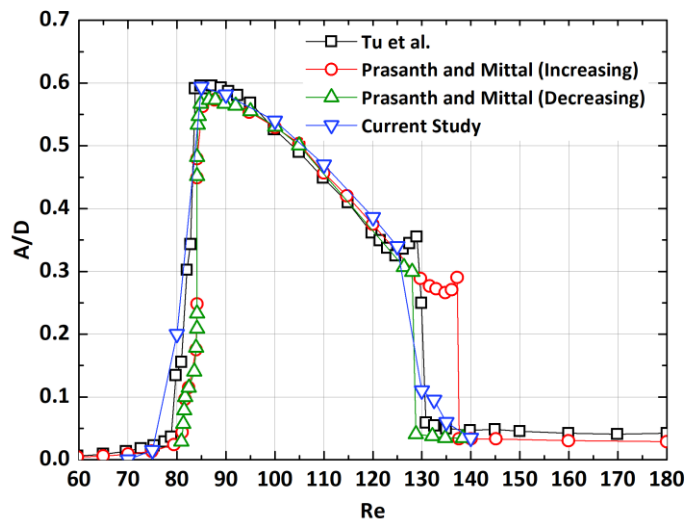

Figure 7 - Variation of statistical values of the cylinder responses with Re (Transverse oscillation amplitude)

The Oscillation amplitude follows the trend; the maximum amplitude was well predicted and there are only minor differences in the beginning and end of the synchronization regime.

Taking into account all the above differences, it can be concluded that the present numerical approach is able to predict the FIV of a cylinder and a downstream flat plate with reasonable accuracy.

4 Results and discussions

The present study includes the FIV of the parallel plates individually and simultaneous vibration of the circular cylinder and downstream plates. To avoid any confusion, the results are divided into two main sections as follows:

4.1 Stationary Cylinder – Vibrating Parallel Plates

In this section, the results of the flow simulation around a stationary cylinder and two freely oscillating parallel flat plates mounted in the wake are presented. Firstly, the amplitude response and secondly, the variation of the hydrodynamic forces are discussed. Finally, the contours of the wake structure are presented from different aspects for a better understanding of the observed phenomena.

4.1.1 Amplitude Response

The vibration amplitude and the frequency ratio of a single plate mounted in the wake centerline and two parallel plates with different vertical offsets are presented in Figure 8.

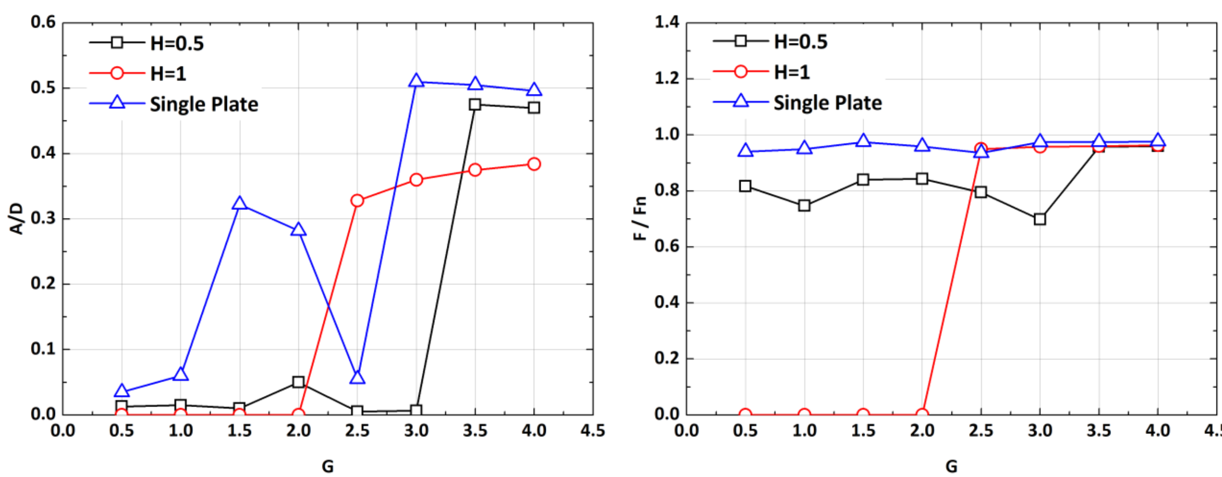

Figure 8 - Oscillation amplitude and frequency ratio of the plates

It is necessary to mention that the authors has decided to assume the motion of cases with a vibration amplitude of A/D<0.001 as zero in the current study. As shown in Figure 8, both of the upper and lower plates behave similarly in terms of amplitude and frequency, and are almost stationary for a range of horizontal distances in the near wake. For the cases with lower vertical distance (H=0.5), no considerable amplitude is observed for G≤3, which is slightly more than a single fixed plate in Hwang's(Hwang et al., 2003) study (G=2.6). When the plates are placed further downstream, the oscillation starts and its amplitude increases to A/D=0.47 for G=3.5. At this point, the frequency ratio, which was about 0.7 in G=3, also jumps and follows the natural frequency of the system for G≥3.5.

At a larger vertical distance (H=1) the plates behave differently. The oscillation disappears completely as the plates approach the cylinder (G≤2) and only begins to oscillate at larger horizontal distances. Although its amplitude increases gradually, but it is lower than in the cases with H=0.5 (18% lower for G=4). The frequency ratio also follows the natural frequency for oscillating cases.

In comparison with a single flat plate, the maximum amplitude which occurs at large values of G, is lower for both of the vertical distances. Although this reduction is not significant for the cases with H=0.5, it falls by more than 20% for the larger vertical gap.

4.1.2 Hydrodynamic forces

The presence of the plates with no oscillation in the near wake usually prevents vortex shedding and results in a symmetric wake. It is also expected that mounting them further has no considerable effect on the cylinder wake structure. In the current study, mounting the parallel plates before a critical value of G≤3 and G≤2 for the vertical spacing of H=0.5 and H=1, respectively, results in considerably lower lift and drag coefficients. According to the results, the jump in the lift coefficient of the cylinder occurs at exactly the same horizontal point where the plates begin to oscillate. After this jump, the CL_{rms} gradually decreases for all configurations and finally reaches the same value at G=4 for both vertical distances (Figure 9).

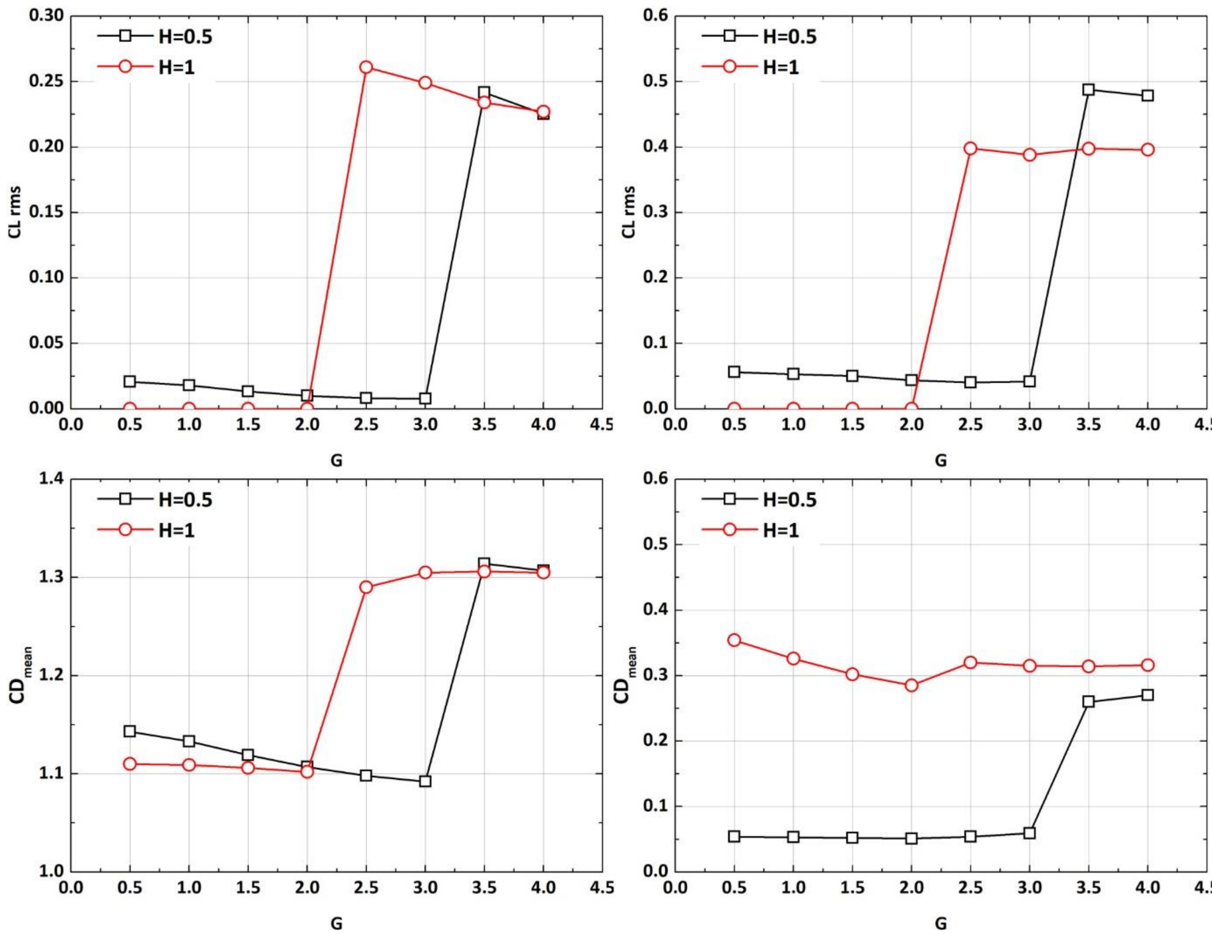

Figure 9 - Variation of root mean square of lift and mean drag coefficients for left) Cylinder right) Parallel Plates

These critical points (G=3-H=0.5, G=2-H=1) can also be seen in the variation of the mean drag coefficient of the cylinder, shown in Figure 9. While the drag coefficient is almost constant for the cases G≤2-H=1, a gradual decrease in Cd_{mean} is observed as the horizontal distance increases up to G=3 for H=0.5.

Since the upper and lower plates behave similarly, only the results for the upper plate are shown in Figure 9. The results show that the jump in the CL_{rms} of the plates is also similar to the corresponding case in the circular cylinder. This phenomenon is also consistent with the jump in the vibration amplitude of the plates.

The variation of the mean drag coefficient is completely different for the plates with different vertical gaps. The shorter vertical gap (H=0.5) is accompanied by a low drag coefficient for the plates with G≤3 and a drastic jump when they are mounted further downstream. The larger vertical gap is fundamentally different and significantly larger in the near wake (up to 7 times for G=0.5). The results show that Cd_{mean} gradually decreases with increasing horizontal distance up to G=2 and then remains almost constant after a small increase for further downstream cases.

4.1.3 Wake Structure

To achieve a better understanding of the system response, a closer look into the near wake structure may be beneficial. Figure 10 shows the variation of the spanwise vorticity for H=0.5 and 1 around their critical horizontal distances at an identical moment ($A/D_{(plates)}$=0).

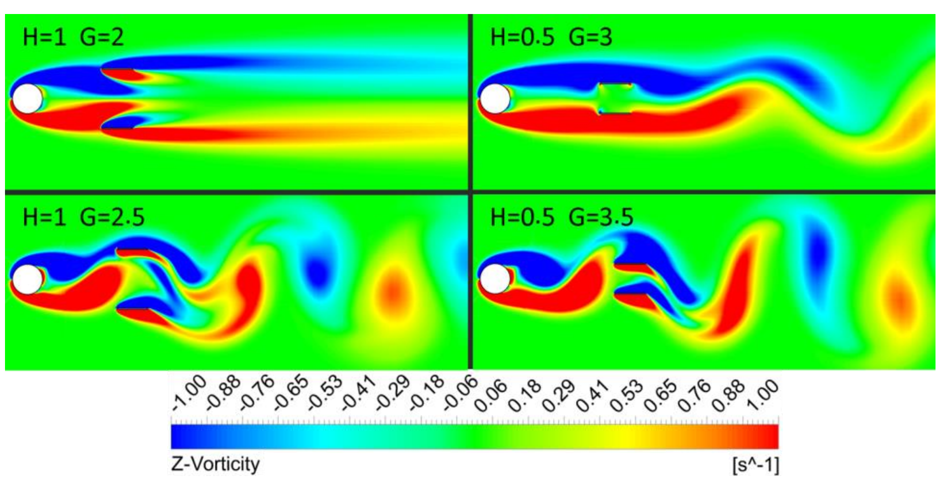

Figure 10 - Spanwise non-dimensional vorticity around the critical horizontal spacing

For the lower vertical gap of H=0.5, when the plates are at G=3, vortex shedding starts further downstream and beyond the parallel plates with a relatively low frequency ratio of F_n=0.7, and a large and symmetric wake forms around the objects. As the parallel plates mount further downstream, vortex shedding occurs between the cylinder and the plates. The new situation which results in an asymmetric flow field around the objects, induces a pressure difference and finally the plates start to oscillate.

Increasing the vertical distance to H=1 results in a shorter vibration-free zone, but the suppression of vortex shedding is even more intense in this region. As shown in the case of G=2-H=1, the presence of parallel plates prevents vortex shedding and leads to secondary, extremely stretched shear layers directly behind the plates. By increasing the horizontal distance, there is again enough space between the cylinder and the plates to form and shed vortices.

The change in vertical distance in fact leads to two major differences in wake structure. The first is the way the parallel plates suppress and prevent vortex shedding. While the larger gap (H=1) keeps the shear layer close together, the smaller one (H=0.5) only keeps them separated and shifts their interaction further downstream. The second difference is in the interaction of shedding vortices and the oscillating parallel plates, which results in slightly narrower and more concentrated circular vortices at H=1.

The length of the recirculation zone was first studied to investigate the effects of varying the Reynolds number on the flow around a bluff body (Zdravkovich, 1997). However, its variation can also be useful in the current study to demonstrate the effects of different configurations on the near wake structure. Figure 11 shows the recirculation zone around the critical horizontal spacings.

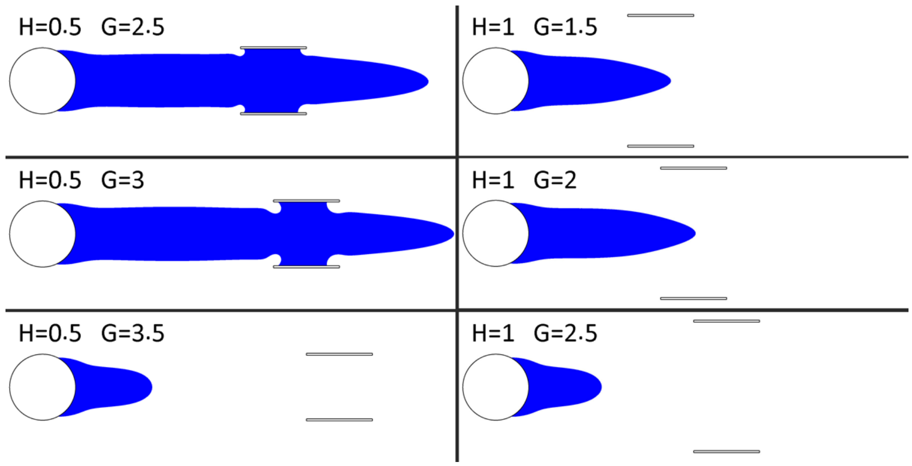

Figure 11 - Variation of Recirculation zone in different configurations

In the cases with a smaller vertical gap (H=0.5), the presence of parallel plates leads to an extended zone of negative mean flow velocity, resulting in long, non-interacting and separated shear layers, as shown in Figure 10. Mounting the plates further downstream (G=3.5) leads to a sudden decrease in R-Z length similar to that of a bare cylinder.

A different pattern is observed in the cases with H=1. The expansion of R-Z takes place again, but it is shorter than those of H=0.5 and extends only to the midpoint of the plates. In this configuration, the sudden change of R-Z occurs at G=2.5.

It is noticeable that the parallel plates only begin to oscillate when they are completely outside the R-Z, and the presence of this region effectively prevents FIMs.

The instantaneous streamline contours for both vertical distances at an identical moment ($A/D_{(plates)}$=0) are shown in Figure 12 to provide a better understanding of the near wake structure.

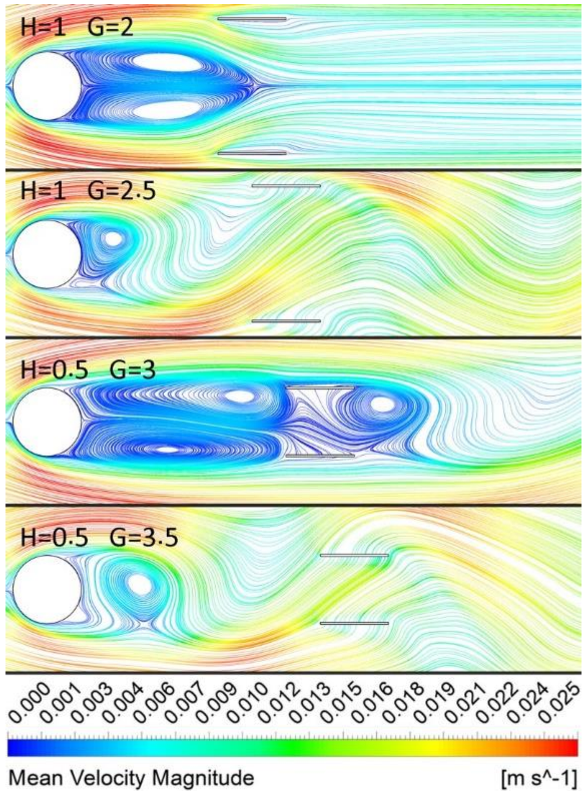

Figure 12 - The instantaneous streamline contours for both of the vertical spacings

For the cases of H=1, mounting the plates up to G≤2 leads to a symmetric wake structure with two stretched bubbles extending to the midpoint of the plates, with a uniform flow downstream and consequently small lift fluctuations for all three objects. Somewhere between G=2 and 2.5, the bubbles suddenly shrink and regular vortex formation and detachment occurs, associated with high lift fluctuations and the start of plates vibration.

The structure of the wake is different in the cases of H=0.5. In these configurations, the cylinder, the bubbles and the parallel plates form a new large and stretched oval shape body and the vortex shedding starts at the end of the plates. Once again by selecting higher values for the horizontal distance (G≥3.5), a regular wake structure appears and the parallel plates start to oscillate by facing shedding vortices.

It seems that the reason for the larger vibration-free region in the cases with H=0.5 is the different method of vortex suppression. The shorter vertical gap and the presence of the parallel plates inside the recirculation zone can suppress vortex shedding for a longer mounting location than the cases with the larger vertical gap in which keeps the separated bubbles together.

As can be seen in Figure 9, the mean drag coefficient in the non-oscillating region is much larger for the cases with a vertical gap of H=1. Figure 12 could also explain the reason for this. The plates are located outside the recirculation zone with low pressure and velocity and are directly exposed to the undisturbed upstream flow. This flow structure results in considerably high drag forces. In contrast, in the cases with the lower vertical gap, the plates are completely inside the low pressure zone, so that a low pressure difference and a low drag coefficient can be expected.

4.2 Simultaneous Free Vibration

In this section, the results of simultaneous free oscillation of a circular cylinder and two parallel flat plates mounted in the wake are presented. First, the amplitude response is discussed, and second, the variation of hydrodynamic forces. Finally, the contours of the wake structure are presented from different angles to provide a better understanding of the observed phenomena.

4.2.1 Amplitude Response

The oscillation amplitude of the cylinder and the parallel plates are shown in Figure 13. Just as in the previous case, the upper and lower plates show similar behavior, so only the results of the upper plate are presented unless otherwise stated.

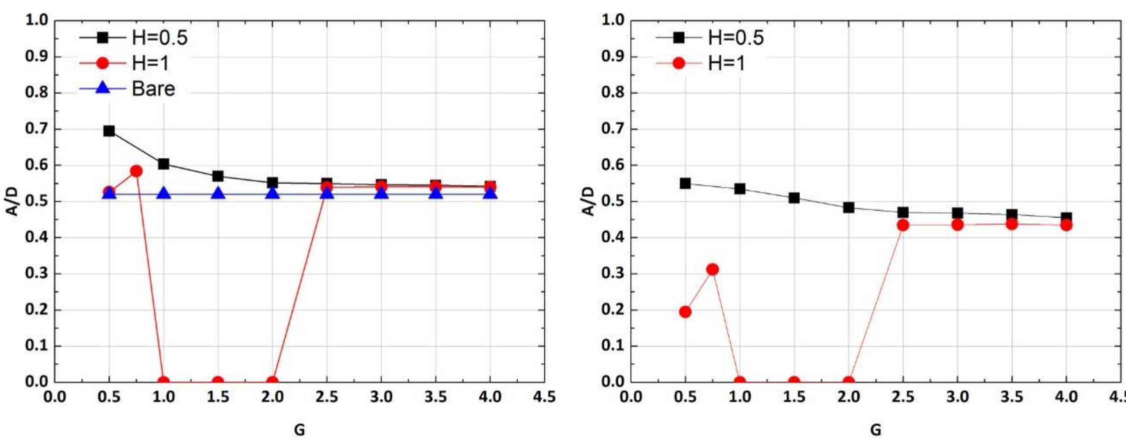

Figure 13 - Oscillation amplitude of the left) cylinder and right) plates

The presence of parallel plates with a vertical spacing of H=0.5 amplifies the vibration amplitude of the cylinder for all configurations, although it is negligible for large horizontal spacings (e.g. G=2-4). The closer the plates are, the more remarkable their effect becomes and the maximum amplitude of the cylinder reaches up to A/D=0.695, which is about 33% higher than that of a bare cylinder.

The response of the cylinder is different for a vertical gap of H=1. While the amplitude of vibration is similar for the large horizontal gaps, it disappears for a range of relatively short G=1-2, which could be due to the suppression of vortex shedding. By decreasing the gap, the cylinder starts to oscillate again for G < 1, with a maximum amplitude close to that of a bare cylinder.

The parallel plates follow an almost similar trend in all cases. For a vertical distance of H=0.5, their amplitude increases gradually as the horizontal distance decreases, reaching its highest amplitude at G=0.5D, which is 20% larger than that of the cases with larger distances (e.g. G=4D). In the cases with the larger vertical distance (H=1), the plates behave similarly to the circular cylinder with a disappearance of the oscillation and a re-growth at the same horizontal distances. The difference, however, is that the amplitude of this configuration is only about half that of the cases with large values of G (G=2.5-4).

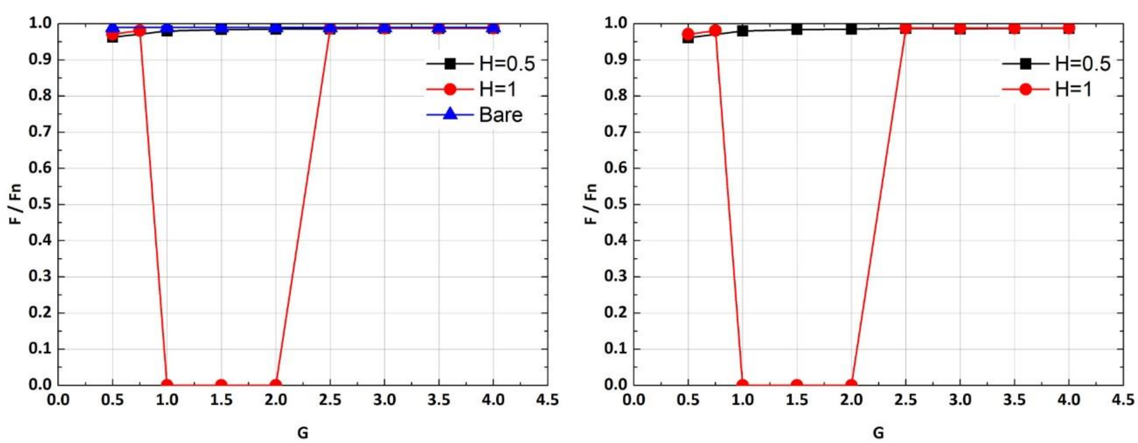

Figure 14 – Frequency ratio of the left) cylinder and right) plates

The variation of the oscillation frequency is similar for both the cylinder and the plates. For a vertical spacing of H=0.5, the cylinder and the plates follow the natural frequency in all configurations. The choice of H=1 leads to a drastic drop in the frequency ratio of the objects for G=1-2, which is consistent with the disappearance of the oscillation (Figure 14).

Figure 15 shows the phase difference between oscillation of the cylinder and the plates. It should be noted that the parallel plates oscillate with the same phase in all the configurations.

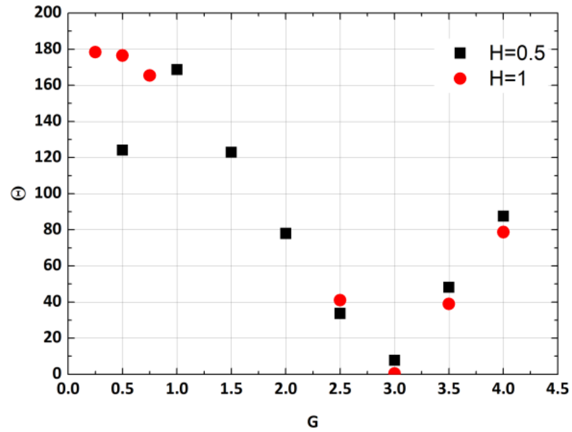

Figure 15 - Oscillation phase difference

According to the results, the phase difference is a function of the horizontal distance and reaches its minimum value at G=3. On the other hand, the maximum difference occurs at small horizontal distances of G=1.

While the phase difference in the cases with H=0.5 decreases as the plates get closer, which is to be expected due to its relation with the horizontal distance, it surprisingly remains almost constant in the cases with a large vertical distance of H=1.

4.2.2 Hydrodynamic Forces

The variation of CL_{rms} of the cylinder also confirms its vibration behavior. As the plates get closer to the cylinder, the CL_{rms} value increases at H=0.5 and reaches up to 0.62, which is about 2.5 times higher than large horizontal distances (Figure 16).

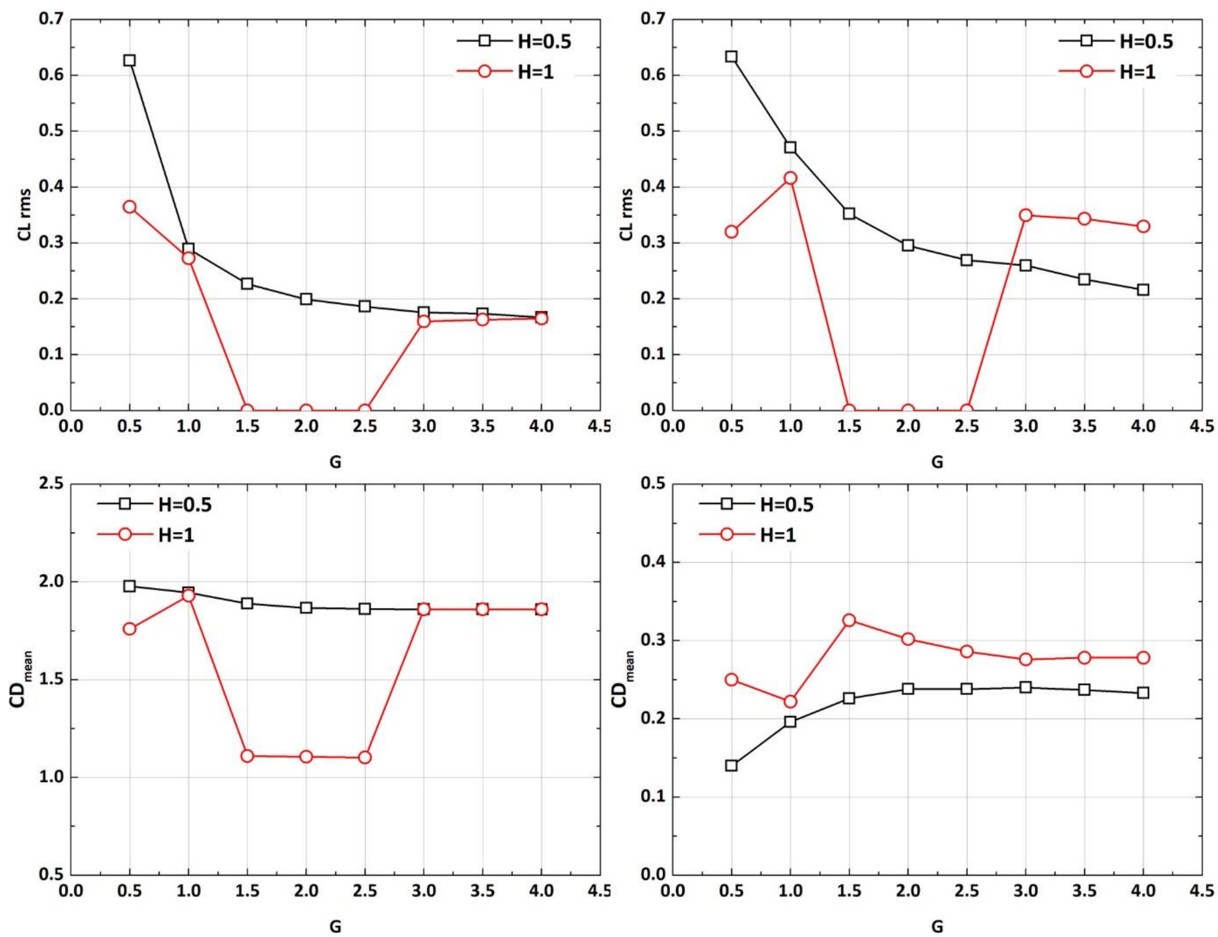

Figure 16 – Hydrodynamic forces on simultaneous oscillation left) cylinder, right) plates

For the cases of H=1, the sudden drop of CL_{rms} occurs at the expected horizontal gaps. While it rises again at small Spacings of G≤1, its amplitude is considerably lower than for the cases with H=0.5, especially for G=0.5.

An almost similar pattern with the same rise and fall is found in parallel plates. When the horizontal gap is large (G > 2.5), the lift force is slightly less in the cases with H=0.5, but gradually increases as the gap decreases, and is about twice that of the similar case with H=1.

The mean drag coefficient of the circular cylinder is almost the same for large values of G for both vertical distances. While CD_{mean} increases slightly for the cases with H=0.5 as the plates approach, it falls for a range of distances including G=1-2 and finally rises again for G < 1, which is consistent with the fall and rise of CLrms and the oscillation amplitude.

The plates with the larger vertical gap of H=1 face with a relatively larger mean drag coefficient in every horizontal distance. Relatively large values of G are accompanied by a nearly constant Cdmean. By decreasing the horizontal gap, gradually decreases for the cases with H=0.5, but behaves differently for H=1 with a temporary rise and then a fall.

As mentioned above, the amplitude of vibration of the circular cylinder at a horizontal gap of G=0.5 is only slightly lower for the vertical gap of H=1, while it decreases significantly (about 65%) for the parallel plates.

The energy transfer from the fluid to the circular cylinder is analyzed for the bare cylinder and that of G=0.5-H=0.5 which has a considerably higher vibration amplitude. The energy transfer rate is defined as $\dot{e} = CL\,.\,\dot{A}/_{D}$ (Li and Ishihara, 2021b). In Figure 17 the variation of vibration amplitude, lift coefficient and energy transfer rate of a bare cylinder and those of case G=0.5-H=0.5 are presented during one cycle of oscillation.

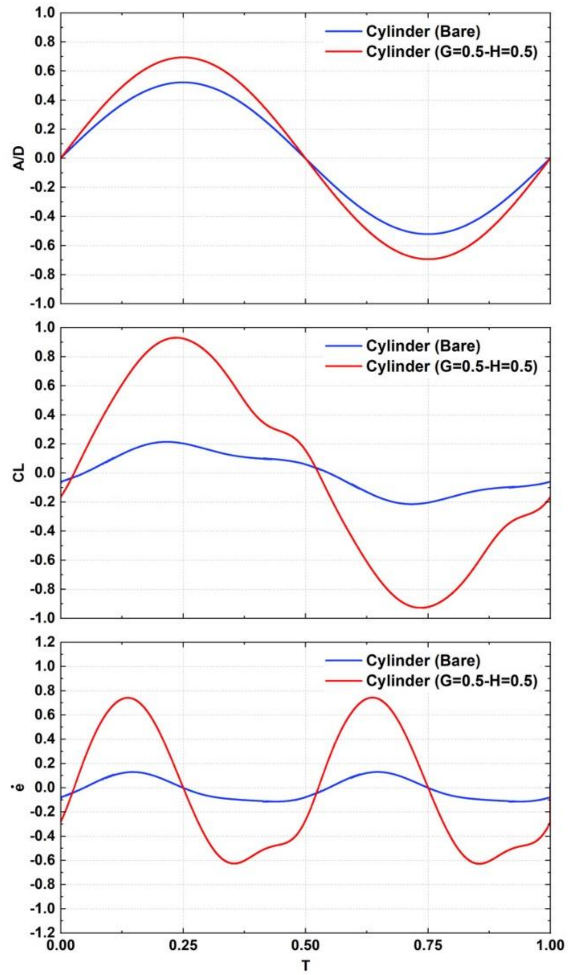

Figure 17) Comparison of vibration amplitude, lift coefficient and energy transfer rate of the bare cylinder and that of G=0.5-H=0.5

According to the results, the cylinder vibration and lift coefficient are in-phase for both of the cases. The lift coefficient in the case of G=0.5-H=0.5 is considerably higher, therefore it results in a higher energy transfer rate and consequently a higher vibration amplitude. The peak of energy transfer rate happens two times in a vibration cycle just before the cylinder reaches its maximum position which results in acceleration of the object.

Figure 18 shows the representative cases of the lift force time histories of the cylinder and the plates for the cases G=0.5-H=0.5 and G=0.5-H=1.

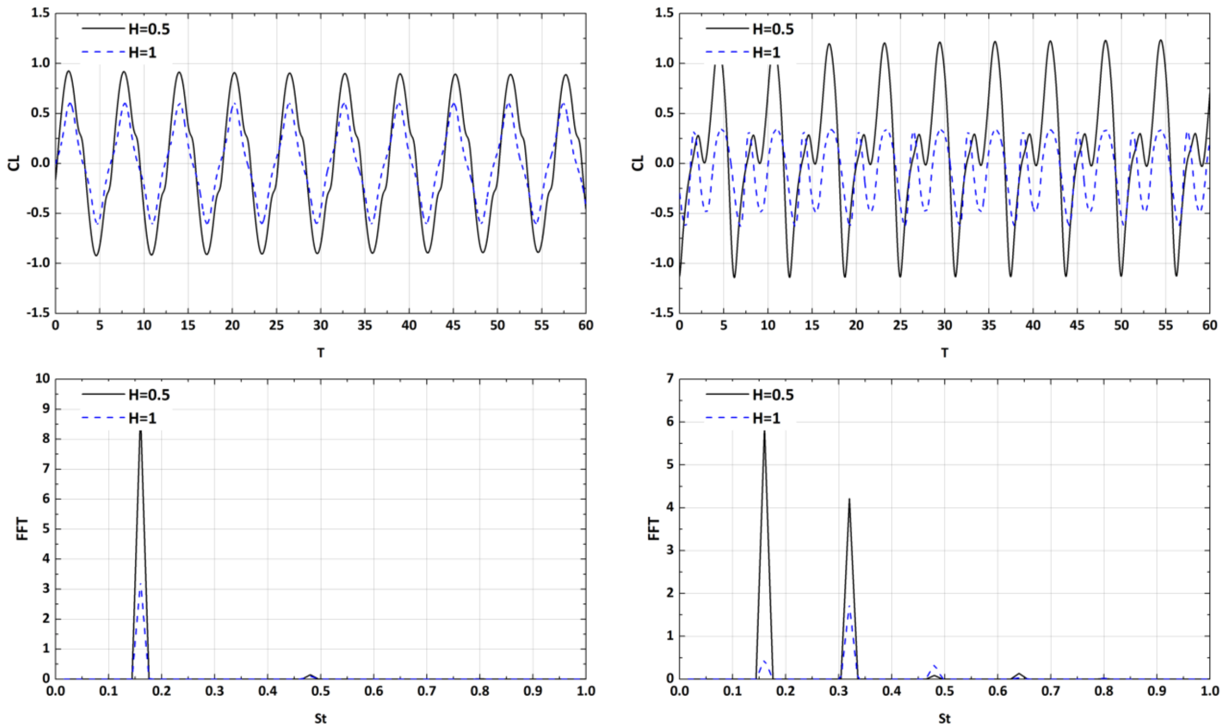

Figure 18 – Time histories of oscillation and lift force coefficient along with FFT plots at G=0.5 for left) Cylinder right) Plates

According to the results, the maximum lift coefficient of the cylinder with H=0.5 is higher and it is easy to find a single dominant frequency for this case, which is equal to its natural frequency. Although the cylinder with H=1 has a lower maximum lift, the dominant frequency is the same. There is also a weak frequency which is twice the natural frequency of the objects and has insignificant effect on the behavior of the cylinder.

For the parallel plates, the dominant frequency is not necessarily equal to the natural one. In the case of H=0.5, two main frequencies are observed, but the lower frequency is still the dominant one. The peak value of the lift coefficient is significantly high and it seems that the second frequency results in amplification of the maximum lift and a small variation in the lift coefficient during an oscillation cycle.

But the lift variation is quite different by increasing the vertical distance to H=1. This configuration also leads to two main frequencies, equal and double the natural frequency, the latter being considered dominant. The variation of the lift coefficient shows a much lower maximum amplitude, confirming the low amplitude of vibration of the plates. It seems that the appearance of the second frequency not only enhances the small variation of lift, but also dampens the maximum amplitude during one cycle of oscillation.

4.2.3 Wake Structure

Figure 19 shows the variation of the spanwise vorticity and the streamlines of the flow for the cases with a vertical gap of H=1.

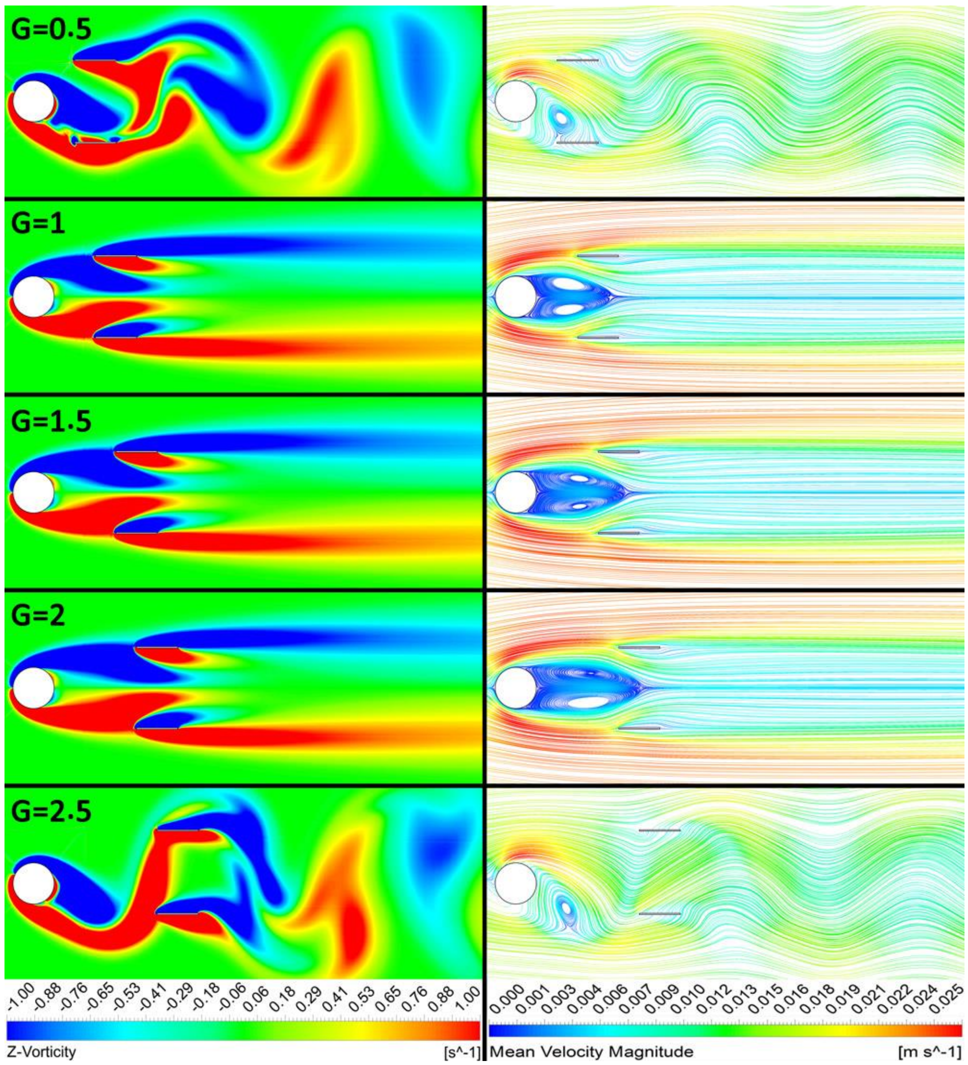

Figure 19 - spanwise non-dimensional vorticity and streamlines of the flow for the cases with a vertical gap of H=1

As mentioned earlier, there is a range of horizontal distance, including G=1-2, at which all objects are almost stationary. When the plates are mounted at G=0.5, their interaction with the shear layers causes the objects to oscillate. When they move slightly downstream, the amplitude suddenly decreases and a symmetric wake structure with two extremely stretched shear layers is formed. This flow structure also occurs as long as G < 2.5. At this point, the vortices form and shed again and a regular wake appears.

Mounting the plates at G=0.5 for both vertical gaps results in oscillating plates but the amplitude of the cases with H=1 is considerably lower. To find an explanation, Figure 20 shows the streamline contours for one cycle of the cylinder oscillation in G=0.5-H=1.

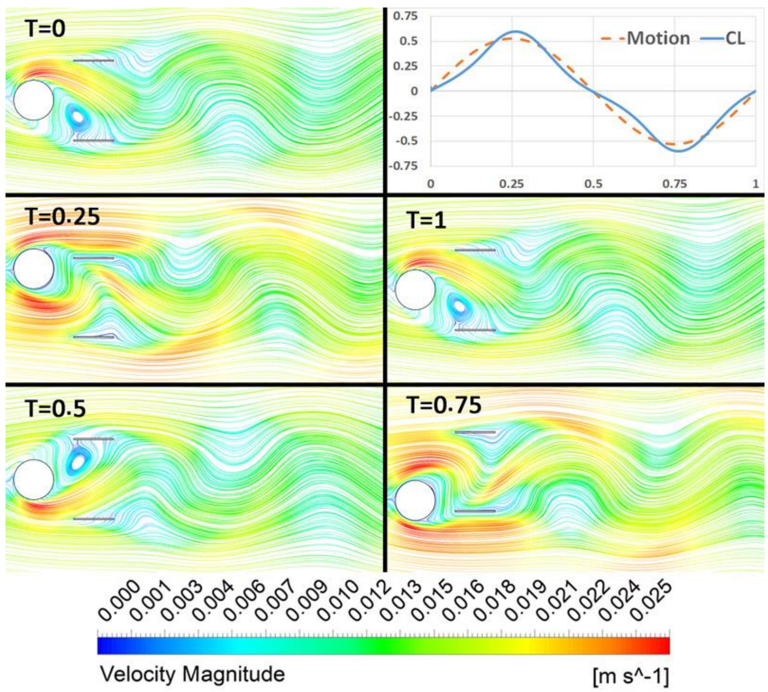

Figure 20 - the streamline contours for one cycle of cylinder for G=0.5-H=1

In the case of G=0.5-H=1, the maximum amplitude of the cylinder during one cycle of oscillation is about 50% of its diameter, which is equal to the oscillation centerline of the plates. Thus, mounting the plates at H=1, results in forming a channel that most part of the shedding vortices pass through it (Figure 20). While this wake structure has no considerable effect on the response of the cylinder, it comes with a lower amplitude for the plates.

This wake structure may also help to find the origin of the second frequency and the reason for its domination for G=0.5-H=1. In Figure 21, the variation of pressure coefficient, as the main source of lift force, is presented in one cycle of plates' oscillation for an identical horizontal gap and different vertical ones. (G=0.5-H=0.5, 1)

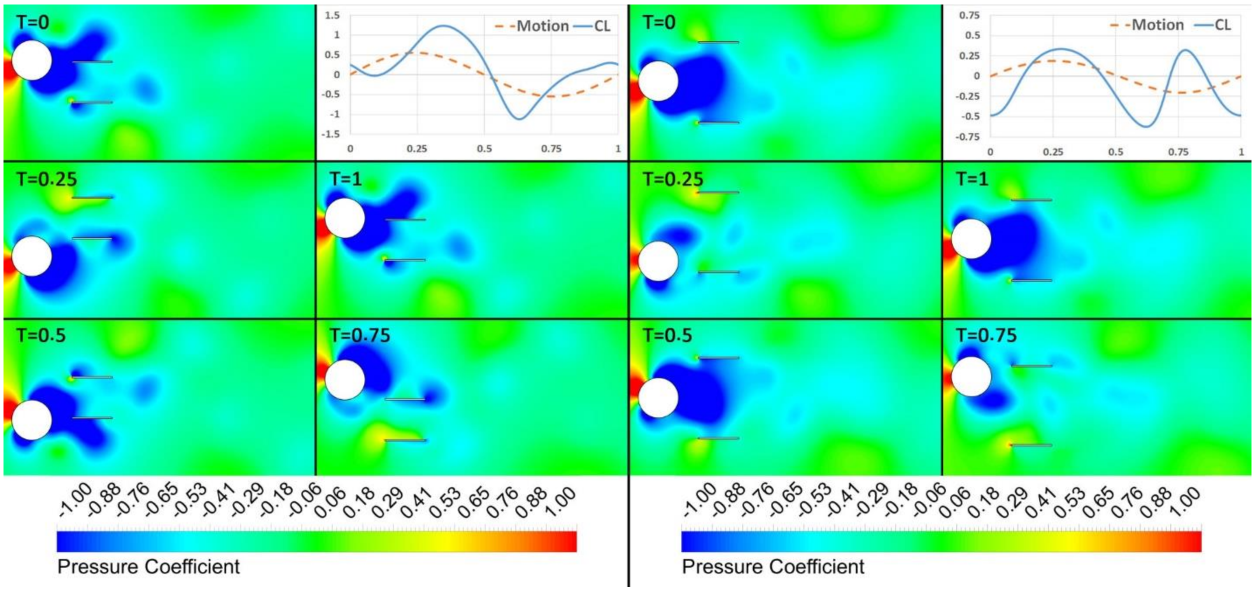

Figure 21 – the distribution of pressure coefficient in cases of G=0.5, Left) H=0.5, Right) H=1

While for the case with a low vertical gap of H=0.5, each plate faces with the shedding vortex of the same side, the upper and lower plate with the upper and lower shedding vortex, respectively, and this interaction only appears ones in an oscillation cycle, this is different for the cases with H=1. As mentioned earlier, the plates make a channel for passing vortices in the case of G=0.5-H=1 that is also visible in Figure 21. Considering a specific plate, for example the upper one, shows that it faces both of the shedding vortices from the upper and lower sides of the cylinder periodically (at T=0 and T=0.5 for the lower and upper vortices, respectively). Since the frequency of this phenomenon is twice that of the vortex shedding of the cylinder, a second dominant frequency equal to 2Fn appears in lift variation. A reduction in maximum lift coefficient and change in the lift dominant frequency changes the system in a way that there will be no longer lock-in phenomena in the response of the plates and the oscillation amplitude falls considerably.

4.2.4 Synchronization Regime

As presented in the last sections, simultaneous vibration may amplify the vibration of all objects depending on their geometry. But to portray an accurate picture of the phenomena, it is necessary to change the reduced velocity and simulate the entire lock-in range for the objects.

The cases with a vertical gap of H=0.5 show better performance by vibrating at every horizontal spacing and even higher vibration amplitude for all objects. Therefore two cases of G=0.5-H=0.5 and G=3-H=0.5 are selected to be studied in a range of Re numbers to cover the entire lock-in regime. The first one is selected because of the higher maximum amplitude and the latter one as a case with negligible effect of the plates on the cylinder and also the lowest motion phase difference between the objects.

Figure 22 presents a comparison between a bare cylinder and cases G=0.5-H=0.5 and G=3-H=0.5. According to the results, when the plates are mounted at G=3, the cylinder amplitude response is generally similar to a bare one and the main difference is at the beginning of the lock-in regime which occurs at a higher Re number of 100 (equivalent to Ur=6). This is accompanied by a gradual decrease up to 120 (U_r=7.2) and then a sudden fall at 130 (U_r=7.8). Mounting the plates at G=0.5 changes the response of the cylinder considerably. The maximum vibration amplitude rises and reaches up to A/D=0.7 which shows at least 20% growth compared with the two other cases. This configuration also widens the lock-in regime and the fall in vibration amplitude is delayed to about Re=200 (U_r=12).

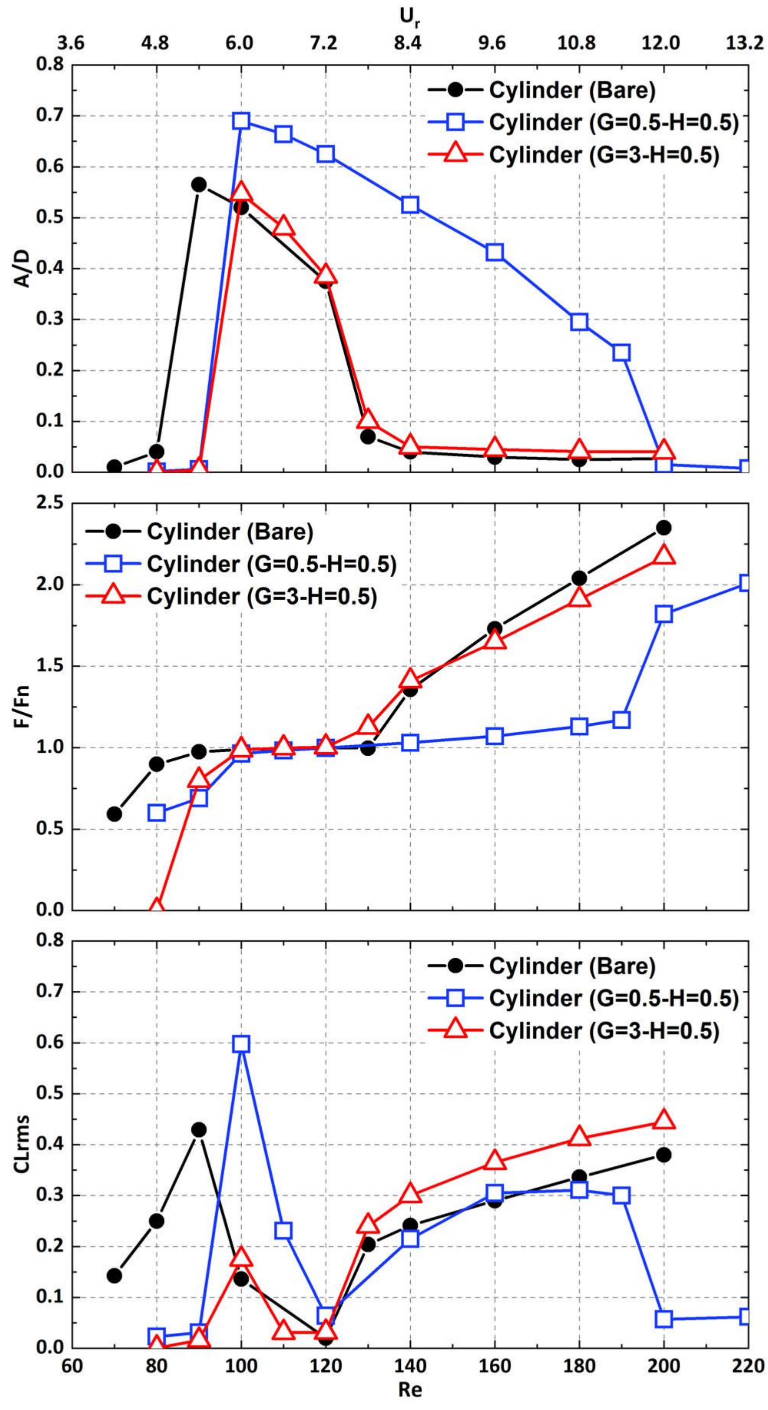

Figure 22 - Variation of Vibrating amplitude, frequency ratio and CLrms of the cylinder for the bare cylinder, G=0.5-H=0.5 and G=3-H=0.5

Variation of frequency ratio confirms the start and end of the synchronization regime at Re=100, 130 respectively for G=3-H=0.5. The lock-in regime extends to higher Re numbers for a shorter gap of G=0.5 which confirms the wider range of Re numbers with a high vibration amplitude.

Although a similar pattern is found in the variation of CLrms for all cases, there are also discrepancies especially before and after the Synchronization regime. Before the start of lock-in, the CL_{rms} is considerably lower for the cases with parallel plates and at a Re number of 200 (Ur=12), the lift of G=0.5-H=0.5 falls significantly while it is still growing for two other cases. These two points have discoursed later.

Similar behavior can be observed for the plates (Figure 23). For both of the configurations, the vibration amplitude jumps at Re=100. It continues with a gradual increase up to Re=120 and drastically falls for Re=130 for G=3. In the case of G=0.5, higher maximum amplitude and a wider lock-in range can be observed. While the rise of vibration amplitude similarly occurs at Re=100, it continues with a temporary increase up to Re=120 and after a gradual decrease, falls at Re=200.

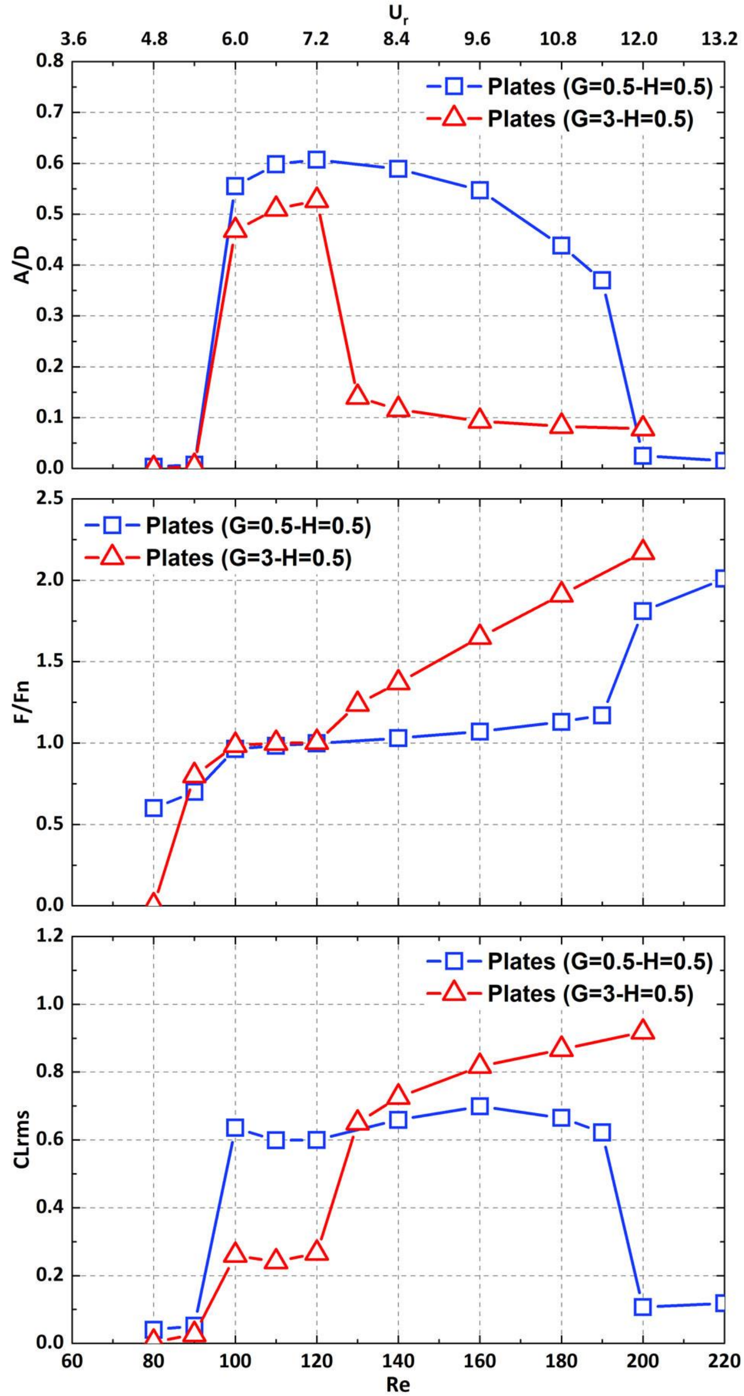

556 **Figure 23 - Variation of Vibrating amplitude, frequency ratio and CLrms of the plates for cases G=0.5-H=0.5 and G=3-H=0.5**

The variation of frequency ratio also confirms the wider range of lock-in regime for a shorter horizontal gap of G=0.5. While a higher CL_{rms} is found by increasing the Re number for G=3, it falls, like the cylinder, at the end of the synchronization range when G=0.5.

To achieve a better understanding of the behavior of the lift force, the variation of spanwise vorticity is presented for the Re numbers 90, and 200 in Figure 24 and Figure 25 respectively.

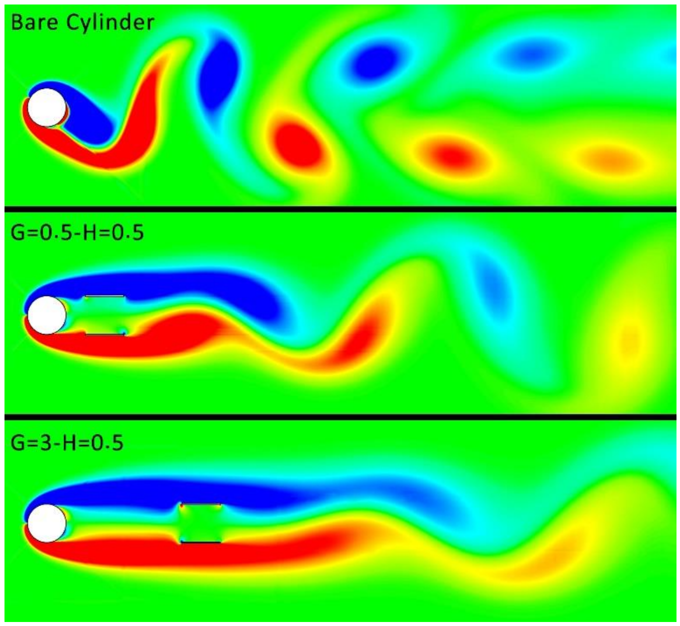

Figure 24 - Spanwise vorticity contours for different configurations at Re=90

As mentioned earlier, the start of lock-in happens at a slightly higher velocity in presence of flat plates. According to Figure 24, the vortex shedding starts further downstream and beyond the plates for G=0.5,3-H=0.5. The shedding frequency is obviously lower for both cases and the lowest one belongs to the case G=3-H=0.5. In this case, the vibrations are smaller than the critical value and are set to zero which is presented in Figure 22 and Figure 23. This flow structure results in a low pressure difference and consequently CL_{rms} for all objects.

By increasing the velocity, CL_{rms} gradually rises after the end of the lock-in regime for the bare cylinder and G=3-H=0.5. But it falls drastically by the end of synchronization for the case of a smaller horizontal gap (G=0.5).

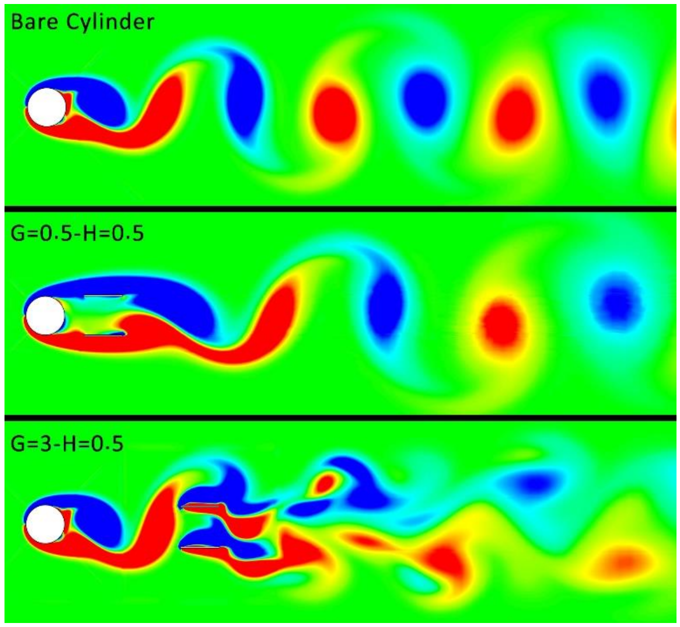

Figure 25 - Spanwise vorticity contours for different configurations at Re=200

Figure 25 presents the spanwise vorticity to reveal the mechanism behind this fall. According to the results, mounting the plates at G=0.5 once again results in a delay in vortex shedding and it occurs beyond the plates which confirms the low amplitude of lift coefficient. When G=3, unlike the Re=90, the vortex shedding happens between the cylinder and the plates, therefore a high value for CL_{rms} is reasonable.

The results of the current sections show that a small horizontal spacing of G=0.5-H=0.5, not only amplifies the maximum vibration amplitude but also widens the lock-in regime for the cylinder and the parallel plates. On the other hand, selecting high horizontal spacing, like G=3, may have no considerable effect on the lock-in regime of each object.

Although further investigation is needed, the higher amplitude and wider lock-in range found in this study, especially in very small horizontal spacing, show that the present concept has a considerable potential to be utilized in the design of an improved energy harvesting system from independent objects in a small area.

5 Conclusion

Numerical simulations were conducted to investigate the effect of two parallel free to vibrate flat plats on the wake structure and vortex-induced vibration of an upstream circular cylinder in different horizontal and vertical spacing at a Re number of 100. The following conclusions are drawn:

1. The response of two freely oscillating parallel plates in the wake of a stationary cylinder depends on both their horizontal and vertical positions. While a decrease in the vertical distance results to a longer non-vibrating horizontal region, it leads to a higher maximum vibration amplitude for the larger horizontal gaps.

2. The wake structure in non-oscillating cases is also related to the vertical distance. The suppression in the cases with H=1 comes with two stretched bubbles extending to the midpoint of the plates and a uniform downstream flow. The vortex suppression for the cases with H=0.5 is due to the fact that the shear layers remain separated and the vortex formation and shedding is shifted to the backside of the plates. Accordingly, the recirculation zone is considerably larger for H=0.5 configurations.

3. When the cylinder and the parallel plates vibrate simultaneously, mounting the plates at H=0.5 results in a considerably higher amplitude of vibration for the cylinder at small horizontal distances. The response of the cylinder in the cases with H=1 is different, it includes oscillation, suppression and finally oscillation again by decreasing the horizontal spacing. The amplitude is also much lower than in the similar case with H=0.5 and is close to a bare cylinder.

4. The effect of vertical spacing has a greater influence on the oscillation amplitude of the plates, especially in close configurations. Increasing the spacing to H=1 not only results in a non-vibrating region, but also leads to an amplitude reduction of 50% for the parallel plates.

5. The main difference at this point is the interaction between the plates, the shear layers, and the shedding vortices. A vertical distance of H=1 results in forming a channel that the vortices flow through it. This phenomenon leads to an amplification of a second frequency in the lift coefficient and a significant reduction in the amplitude of oscillation.

6. A small horizontal spacing with a proper vertical gap, not only may amplify the maximum vibration amplitude but also can widen the lock-in regime for the cylinder and the parallel plates. Although further investigation is needed, the higher amplitude and wider lock-in range found in this study show that the present concept has a considerable potential to be utilized in the design of an improved energy harvesting system from independent objects in a small area.

Acknowledgment

"The authors acknowledge the use of the UCL Grace High Performance Computing Facility (Kathleen@UCL), and associated support services, in the completion of this work."

References

An, X., Song, B., Tian, W., Ma, C., 2018. Design and CFD simulations of a vortex-induced piezoelectric energy converter (VIPEC) for underwater environment. Energies 11, 330.

Apelt, C.J., West, G.S., Szewczyk, A.A., 1973. The effects of wake splitter plates on the flow past a circular cylinder in the range 104< R< 5× 104. J. Fluid Mech. 61, 187–198.

Armandei, M., Fernandes, A.C., 2016. Marine current energy extraction through buffeting. Int. J. Mar. Energy 14, 52–67.

Assi, G.R.S., Bearman, P.W., 2015. Transverse galloping of circular cylinders fitted with solid and slotted splitter plates. J. Fluids Struct. 54, 263–280.

Assi, G.R.S., Bearman, P.W., Tognarelli, M.A., 2014. On the stability of a free-to-rotate short-tail fairing and a splitter plate as suppressors of vortex-induced vibration. Ocean Eng. 92, 234–244. https://doi.org/https://doi.org/10.1016/j.oceaneng.2014.10.007

Bearman, P.W., 1984. Vortex shedding from oscillating bluff bodies. Annu. Rev. Fluid Mech. 16, 195–222.

Chen, W.-L., Xin, D.-B., Xu, F., Li, H., Ou, J.-P., Hu, H., 2013. Suppression of vortex-induced vibration of a circular cylinder using suction-based flow control. J. Fluids Struct. 42, 25–39. https://doi.org/https://doi.org/10.1016/j.jfluidstructs.2013.05.009

Dehkordi, B.G., Jafari, H.H., 2010. On the suppression of vortex shedding from circular cylinders using detached short splitter-plates. J. Fluids Eng. 132.

Facchinetti, M.L., De Langre, E., Biolley, F., 2004. Coupling of structure and wake oscillators in vortex-induced vibrations. J. Fluids Struct. 19, 123–140.

Gerrard, J.H., 1966. The mechanics of the formation region of vortices behind bluff bodies. J. Fluid Mech.

25, 401–413.

He, T., Zhou, D., Bao, Y., 2012. Combined interface boundary condition method for fluid–rigid body interaction. Comput. Methods Appl. Mech. Eng. 223, 81–102.

Hwang, J.-Y., Yang, K.-S., Sun, S.-H., 2003. Reduction of flow-induced forces on a circular cylinder using a detached splitter plate. Phys. Fluids 15, 2433–2436.

Ishihara, T., Li, T., 2020. Numerical study on suppression of vortex-induced vibration of circular cylinder by helical wires. J. Wind Eng. Ind. Aerodyn. 197, 104081.

Jiang, H., Cheng, L., Draper, S., An, H., Tong, F., 2016. Three-dimensional direct numerical simulation of wake transitions of a circular cylinder. J. Fluid Mech. 801, 353.

Kawai, H., 1990. A discrete vortex analysis of flow around a vibrating cylinder with a splitter plate. J. Wind Eng. Ind. Aerodyn. 35, 259–273.

Kravchenko, A.G., Moin, P., 1998. B-spline methods and zonal grids for numerical simulations of turbulent flows. Report No. TF-73, Department of Mechanical Engineering.

Kumar, D., Singh, A.K., Sen, S., 2018. Identification of response branches for oscillators with curved and straight contours executing VIV. Ocean Eng. 164, 616–627.

Kwon, K., Choi, H., 1996. Control of laminar vortex shedding behind a circular cylinder using splitter plates. Phys. Fluids 8, 479–486.

Li, T., Ishihara, T., 2021a. Numerical study on wake galloping of tandem circular cylinders considering the effects of mass and spacing ratios. J. Wind Eng. Ind. Aerodyn. 210, 104536.

Li, T., Ishihara, T., 2021b. Numerical study on vortex-induced vibration of circular cylinder with two-degree-of-freedom and geometrical nonlinear system. J. Fluids Struct. 107, 103415.

Li, Y., Zhang, R., Shock, R., Chen, H., 2009. Prediction of vortex shedding from a circular cylinder using a volumetric Lattice-Boltzmann boundary approach. Eur. Phys. J. Spec. Top. 171, 91–97.

Liang, S., Wang, J., Hu, Z., 2018. VIV and galloping response of a circular cylinder with rigid detached splitter plates. Ocean Eng. 162, 176–186.

Nakamura, Y., Hirata, K., Kashima, K., 1994. Galloping of a circular cylinder in the presence of a splitter plate. J. Fluids Struct. 8, 355–365.

Nguyen, V.-T., Nguyen, H.H., 2016. Detached eddy simulations of flow induced vibrations of circular cylinders at high Reynolds numbers. J. Fluids Struct. 63, 103–119.

Ozkan, G.M., Firat, E., Akilli, H., 2017. Passive flow control in the near wake of a circular cylinder using attached permeable and inclined short plates. Ocean Eng. 134, 35–49. https://doi.org/https://doi.org/10.1016/j.oceaneng.2017.02.014

Ozono, S., 1999. Flow control of vortex shedding by a short splitter plate asymmetrically arranged downstream of a cylinder. Phys. Fluids 11, 2928–2934.

Park, J., Kwon, K., Choi, H., 1998. Numerical solutions of flow past a circular cylinder at Reynolds numbers up to 160. KSME Int. J. 12, 1200–1205.

Posdziech, O., Grundmann, R., 2007. A systematic approach to the numerical calculation of fundamental quantities of the two-dimensional flow over a circular cylinder. J. Fluids Struct. 23, 479–499.

Prasanth, T.K., Behara, S., Singh, S.P., Kumar, R., Mittal, S., 2006. Effect of blockage on vortex-induced vibrations at low Reynolds numbers. J. Fluids Struct. 22, 865–876.

Prasanth, T.K., Mittal, S., 2009. Vortex-induced vibration of two circular cylinders at low Reynolds number. J. Fluids Struct. 25, 731–741.

Prasanth, T.K., Mittal, S., 2008. Vortex-induced vibrations of a circular cylinder at low Reynolds numbers. J. Fluid Mech. 594, 463.

Qu, L., Norberg, C., Davidson, L., Peng, S.-H., Wang, F., 2013. Quantitative numerical analysis of flow past a circular cylinder at Reynolds number between 50 and 200. J. Fluids Struct. 39, 347–370.

Quadrante, L.A.R., Nishi, Y., 2014. Amplification/suppression of flow-induced motions of an elastically mounted circular cylinder by attaching tripping wires. J. Fluids Struct. 48, 93–102. https://doi.org/https://doi.org/10.1016/j.jfluidstructs.2014.02.018

Roshko, A., 1954. On the drag and shedding frequency of two-dimensional bluff bodies.

Rostami, A.B., Armandei, M., 2017. Renewable energy harvesting by vortex-induced motions: Review and benchmarking of technologies. Renew. Sustain. Energy Rev. 70, 193–214.

Sarpkaya, T., 2004. A critical review of the intrinsic nature of vortex-induced vibrations. J. Fluids Struct. 19, 389–447.

Sarpkaya, T., 1979. Vortex-induced oscillations: a selective review.

Soumya, S., Prakash, K.A., 2017. Effect of splitter plate on passive control and drag reduction for fluid flow past an elliptic cylinder. Ocean Eng. 141, 351–374. https://doi.org/https://doi.org/10.1016/j.oceaneng.2017.06.034

Stålberg, E., Brüger, A., Lötstedt, P., Johansson, A. V, Henningson, D.S., 2006. High order accurate solution of flow past a circular cylinder. J. Sci. Comput. 27, 431–441.

Stappenbelt, B., 2010. Splitter-plate wake stabilisation and low aspect ratio cylinder flow-induced vibration mitigation. Int. J. Offshore Polar Eng. 20.

Sui, J., Wang, J., Liang, S., Tian, Q., 2016. VIV suppression for a large mass-damping cylinder attached with helical strakes. J. Fluids Struct. 62, 125–146. https://doi.org/https://doi.org/10.1016/j.jfluidstructs.2016.01.005

Sun, X., Suh, C.S., Ye, Z.-H., Yu, B., 2020. Dynamics of a circular cylinder with an attached splitter plate in laminar flow: A transition from vortex-induced vibration to galloping. Phys. Fluids 32, 27104.

Tu, J., Zhou, D., Bao, Y., Ma, J., Lu, J., Han, Z., 2015. Flow-induced vibrations of two circular cylinders in tandem with shear flow at low Reynolds number. J. Fluids Struct. 59, 224–251.

Wang, H., Zhai, Q., Hou, J., Xia, L., 2018a. Numerical Investigation on the Vortex-Induced Vibration of a Flexible Plate behind a Circular Cylinder. J. Coast. Res. 85, 1326–1330.

Wang, H., Zhai, Q., Zhang, J., 2018b. Numerical study of flow-induced vibration of a flexible plate behind a circular cylinder. Ocean Eng. 163, 419–430.

White, F.M., 1994. Fluid Mechanics, McGraw-Hill. New York.

Williamson, Charles H K, 1996. Vortex dynamics in the cylinder wake. Annu. Rev. Fluid Mech. 28, 477–539.

Williamson, C H K, 1996. Three-dimensional wake transition, in: Advances in Turbulence VI. Springer, pp. 399–402.

Williamson, C.H.K., Govardhan, R., 2004. Vortex-induced vibrations. Annu. Rev. Fluid Mech. 36, 413–455.

Wu, J., Shu, C., Zhao, N., 2014. Numerical investigation of vortex-induced vibration of a circular cylinder with a hinged flat plate. Phys. Fluids 26, 63601.

Zdravkovich, M.M., 1997. Flow around Circular Cylinders: A Comprehensive Guide through Flow Phenomena. Exp. Appl.

Zhu, H., Gao, Y., 2017. Vortex-induced vibration suppression of a main circular cylinder with two rotating control rods in its near wake: Effect of the rotation direction. J. Fluids Struct. 74, 469–491.

https://doi.org/https://doi.org/10.1016/j.jfluidstructs.2017.07.004

Zhu, H., Li, G., Wang, J., 2020. Flow-induced vibration of a circular cylinder with splitter plates placed upstream and downstream individually and simultaneously. Appl. Ocean Res. 97, 102084.

Zhu, H., Liu, W., 2020. Flow control and vibration response of a circular cylinder attached with a wavy plate. Ocean Eng. 212, 107537. https://doi.org/https://doi.org/10.1016/j.oceaneng.2020.107537

Zhu, H., Yao, J., 2015. Numerical evaluation of passive control of VIV by small control rods. Appl. Ocean Res. 51, 93–116. https://doi.org/https://doi.org/10.1016/j.apor.2015.03.003